applied sciences

MDPI

Supplementary Material

Characterization of charge sharing

Viona S. K. Yokhana [1], Benedicta D. Arhatari [2,1,*] and Brian Abbey [1,3,*]

[1] Department of Mathematical and Physical Sciences, School of Engineering, Computing and Mathematical Sciences, Bundoora, VIC 3086, Australia; 17502317@students.latrobe.edu.au
[2] Australian Synchrotron, ANSTO, Clayton 3168, Australia
[3] La Trobe Institute for Molecular Science, La Trobe University, Bundoora VIC 3086 Australia

* Correspondence: arhatarb@ansto.gov.au or b. abbey@latrobe.edu.au

Prior to quantitatively analysing the PiXirad data the images need to be corrected to account for the effects of charge sharing. Charge sharing occurs when the signal associated with a single photon is spread over multiple pixels [1,2]. There are several interconnected phenomena which determine the degree of charge sharing, but the end result is that there is an apparently higher number of counts within the low energy region of the spectrum compared to the higher energy region [3]. Charge sharing is more complex to model when using polychromatic X-ray sources compared to the monochromatic case and can lead to apparent distortions of the detected X-ray spectrum [4].

To characterize charge sharing in the PiXirad detector, we need to quantitatively compare the experimentally measured transmitted intensity (which is affected by charge sharing) to the simulated one (which is not affected by charge sharing) for a well-characterized sample. Here we present the results of charge sharing calibration using the HA400 insert embedded in epoxy. Provided the PiXirad image contains a region without the sample (i.e. just air) calibration to correct for charge sharing only requires a single image per energy threshold value. Measurement of the intensity through the well-characterised sample and through air as a function of the PiXirad energy threshold is used to quantify any differences in the response of the detector due to charge sharing. Without correction these differences could result in an inaccurate measurement of the linear attenuation coefficient.

Characterization of the detector response through air (no sample) was carried out by simulating the expected signal using the X-ray source spectrum (measured with the XR-100T-CdTe AMPTEK detector) for the different energy threshold values. This provides an estimate of the 'ideal' flatfield intensity, $I_{o,E_{th}}^{sim}$, which is free from the effects of charge sharing. Based on calibration experiments conducted using inserts of varying density (HA400, HA800, and HA1200) the following empirically derived formula was used to obtain the correct value for the transmitted intensity $I_{E_{th}}^{cor}(x,y)$ measured using the PiXirad detector:

$$I_{E_{th}}^{cor}(x,y) = I_{o,E_{th}}^{sim} - \frac{I_{o,E_{th}}^{sim}}{K_{E_{th}}}\left[1 - \frac{I_{E_{th}}^{exp}(x,y)}{I_{o,E_{th}}^{exp}}\right] \quad \text{(S1)}$$

where the subscript, E_{th}, indicates the depedance on the energy threshold value, x and y indicate the position on the 2D detector, and $K_{E_{th}}$ is a fitting parameter which is obtained from the best fit of Eq. S1 to the simulated intensity for the calibration sample, i.e. $I_{E_{th}}^{cor}(x,y) = I_{cal,E_{th}}^{sim}(x,y)$. The values for the ratio $K_{E_{th}}$ for a tube voltage of 40 kVp using the HA400 calibration sample (which has a similar density to mouse bone) are shown in Fig. S1. These values were used to generate the corrected intensity for separation of soft tissue from bone for the mouse hand presented in the paper (Fig. 8). Note that in the absence of any charge sharing, $K_{E_{th}} = 1$ and $I_{o,E_{th}}^{exp} = I_{o,E_{th}}^{sim}$, such that the RHS of Eq. S1 reduces to $I_{E_{th}}^{exp}(x,y)$, the measured intensity through the sample. Since $K_{E_{th}}$ varies as a function of

sample composition, but is assumed to be independent of sample thickness, the results from the calibration measurements can be used to separate any material of similar density for an unknown sample. If a different material needs to be separated the charge sharing calibration measurements to determine $K_{E_{th}}$ as a function of energy threshold should be repeated.

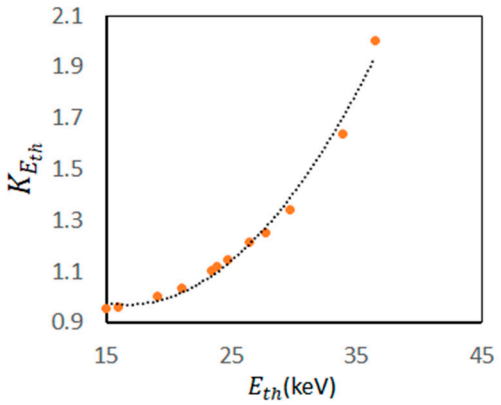

Figure S1. Fitting parameter $K_{E_{th}}$ which characterizes the degree of charge sharing as a function of energy threshold for the HA400 calibration sample.

The values for the ratio $K_{E_{th}}$ for a tube voltage of 80 kVp using the HA800 and HA1200 calibration samples are provided in Table S1. These values are used to correct the charge sharing effect to generate Figure 7(e – f) presented in the paper.

Table S1. Values for the ratio $K_{E_{th}}$ for a tube voltage of 80 kVp.

Threshold energy (keV)	$K_{E_{th}}$	
	HA800	HA1200
E_1 = 16.0	0.971	0.982
E_2 = 21.1	1.009	1.019
E_3 = 23.9	1.046	1.059
E_4 = 29.7	1.089	1.105

The corresponding energy resolution of the PiXirad detector is presented in Figure S2.

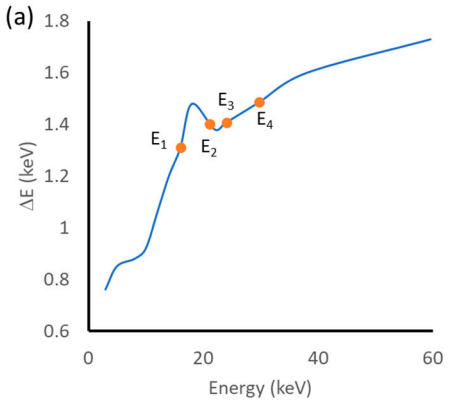

(b)

E (keV) exp.	ΔE (keV)	$\Delta E/E$ (%)	E (keV) sim.
E_1=16.0	1.31	8.1	16
E_2=21.1	1.40	6.4	22
E_3=23.9	1.41	5.9	24
E_4=29.7	1.49	5.0	30

Figure S2. (a) Energy resolution of the PiXirad detector as a function of energy. Data taken from A. Vincenzi et al. [5]. The position of the experimental energy thresholds are indicated by the orange circles. (b) Corresponding energy resolution values for each of the four experimental energy threshold values extrapolated from (a).

A schematic diagram providing an overview of the simulations is presented in Figure S3.

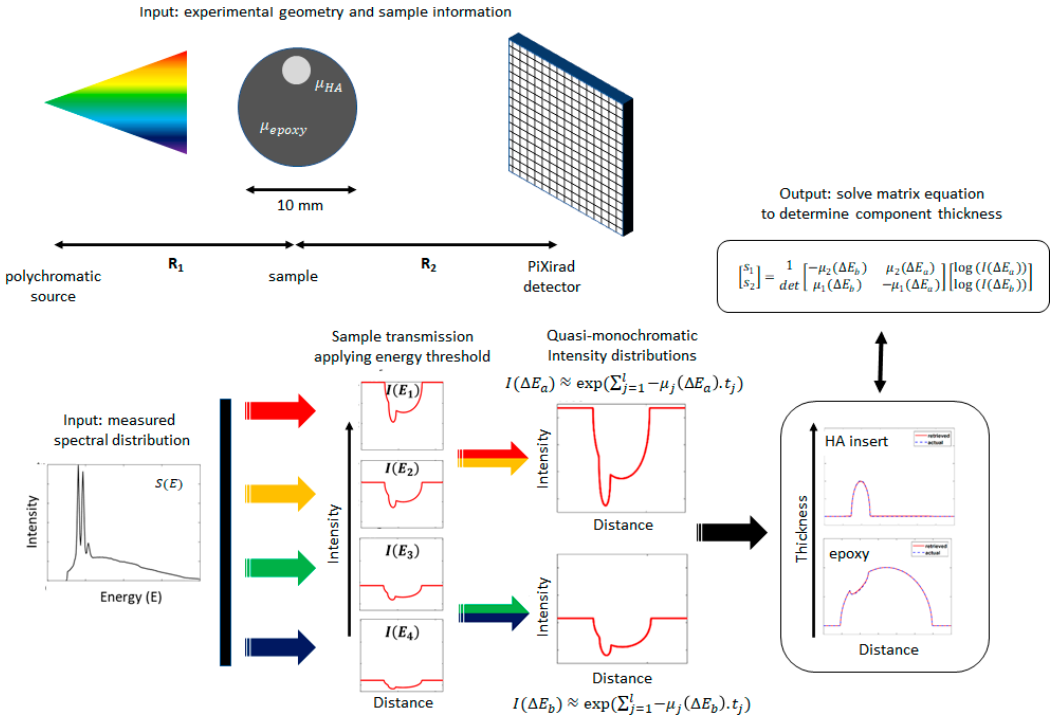

Figure S3. Schematic diagram showing the key steps in the forward simulation and subsequent retrieval of epoxy and HA insert components. All simulations were performed using MATLAB.

References

1. Delogu, P.; Oliva, P.; Bellazzini, R.; Brez, A.; de Ruvo, P.L.; Minuti, M.; Pinchera, M.; Spandre, G.; Vincenzi, A. Characterization of Pixirad-1 photon counting detector for X-ray imaging. *J. Instrum.* **2016**, *11*, P01015-P01015, doi:10.1088/1748-0221/11/01/p01015.
2. Taguchi, K.; Iwanczyk, J.S. Vision 20/20: Single photon counting x-ray detectors in medical imaging. *Med. Phys.* **2013**, *40*, 100901, doi:10.1118/1.4820371.
3. Vincenzi, A.; Ruvo, P.L.d.; Delogu, P.; Bellazzini, R.; Brez, A.; Minuti, M.; Pinchera, M.; Spandre, G. Energy characterization of PiXirad-1 photon counting detector system. *Journal of Instrumentation* **2015**, *10*, C04010.
4. Taguchi, K. Energy-sensitive photon counting detector-based X-ray computed tomography. *Radiological Physics and Technology* **2017**, *10*, 8-22, doi:10.1007/s12194-017-0390-9.
5. Vincenzi, A.; De Ruvo, P.; Delogu, P.; Bellazzini, R.; Brez, A.; Minuti, M.; Pinchera, M.; Spandre, G. Energy characterization of Pixirad-1 photon counting detector system. *Journal of Instrumentation* **2015**, *10*, C04010.